Planck early results

Astronomy & Astrophysics

Special feature

Planck early results. XXVI. Detection with *Planck* and confirmation by *XMM-Newton* of PLCK G266.6–27.3, an exceptionally X-ray luminous and massive galaxy cluster at *z* ∼ 1[⋆]

Planck Collaboration: N. Aghanim[50], M. Arnaud[64], M. Ashdown[62,4], F. Atrio-Barandela[14], J. Aumont[50], C. Baccigalupi[73], A. Balbi[31], A. J. Banday[82,7,68], R. B. Barreiro[58], J. G. Bartlett[3,60], E. Battaner[84], K. Benabed[51,80], A. Benoît[49], J.-P. Bernard[82,7], M. Bersanelli[28,44], R. Bhatia[5], H. Böhringer[69], A. Bonaldi[61], J. R. Bond[6], S. Borgani[29,42], J. Borrill[67,76], F. R. Bouchet[51,80], M. L. Brown[4,62], C. Burigana[43], P. Cabella[31], C. M. Cantalupo[67], B. Cappellini[44], P. Carvalho[4], A. Catalano[3,63], L. Cayón[22], L.-Y. Chiang[54], C. Chiang[21], G. Chon[69,4], P. R. Christensen[70,32], E. Churazov[68,75], D. L. Clements[47], S. Colafrancesco[41], S. Colombi[51,80], B. P. Crill[60,71], F. Cuttaia[43], A. Da Silva[10], H. Dahle[56,9], L. Danese[73], O. D.'Arcangelo[59], R. J. Davis[61], P. de Bernardis[27], G. de Gasperis[31], G. de Zotti[40,73], J. Delabrouille[3], J.-M. Delouis[51,80], J. Démoclès[64], F.-X. Désert[45], C. Dickinson[61], J. M. Diego[58], H. Dole[50], S. Donzelli[44,56], O. Doré[60,8], M. Douspis[50], X. Dupac[36], G. Efstathiou[55], T. A. Enßlin[68], H. K. Eriksen[56], F. Finelli[43], I. Flores-Cacho[57,33], O. Forni[82,7], P. Fosalba[52], M. Frailis[42], E. Franceschi[43], S. Fromenteau[3,50], S. Galeotta[42], K. Ganga[3,48], R. T. Génova-Santos[57,33], M. Giard[82,7], J. González-Nuevo[73], R. González-Riestra[35], K. M. Górski[60,85], A. Gregorio[29], A. Gruppuso[43], F. K. Hansen[56], D. Harrison[55,62], P. Heinämäki[79], C. Hernández-Monteagudo[68,11], S. R. Hildebrandt[8,65,57], E. Hivon[51,80], M. Hobson[4], G. Hurier[65], A. H. Jaffe[47], W. C. Jones[21], M. Juvela[20], E. Keihänen[20], R. Keskitalo[60,20], T. S. Kisner[67], R. Kneissl[34,5], H. Kurki-Suonio[20,39], G. Lagache[50], A. Lähteenmäki[1,39], J.-M. Lamarre[63], A. Lasenby[4,62], C. R. Lawrence[60], M. Le Jeune[3], S. Leach[73], R. Leonardi[36], C. Leroy[50,82,7], A. Liddle[19], P. B. Lilje[56,9], M. López-Caniego[58], G. Luzzi[66], J. F. Macías-Pérez[65], D. Maino[28,44], N. Mandolesi[43], F. Marleau[16], E. Martínez-González[58], S. Masi[27], S. Matarrese[26], P. Mazzotta[31], P. R. Meinhold[24], A. Melchiorri[27], J.-B. Melin[12], L. Mendes[36], A. Mennella[28,42], M.-A. Miville-Deschênes[50,6], A. Moneti[51,80], L. Montier[82,7], G. Morgante[43], D. Mortlock[47], D. Munshi[74,55], P. Naselsky[70,32], P. Natoli[30,2,43], J. Nevalainen[20,38], H. U. Nørgaard-Nielsen[13], F. Noviello[50], D. Novikov[47], I. Novikov[70], I. J. O'Dwyer[60], S. Osborne[77], R. Paladini[48], F. Pasian[42], G. Patanchon[3], T. J. Pearson[8,48], O. Perdereau[66], L. Perotto[65], F. Perrotta[73], F. Piacentini[27], E. Pierpaoli[18], R. Piffaretti[64,12], P. Platania[59], E. Pointecouteau[82,7], G. Polenta[2,41], N. Ponthieu[50], L. Popa[53], T. Poutanen[39,20,1], G. W. Pratt[64], G. Prézeau[8,60], S. Prunet[51,80], J.-L. Puget[50], J. P. Rachen[68], R. Rebolo[57,33], M. Reinecke[68], C. Renault[65], S. Ricciardi[43], T. Riller[68], I. Ristorcelli[82,7], G. Rocha[60,8], J. A. Rubiño-Martín[57,33], E. Saar[78], M. Sandri[43], G. Savini[72], B. M. Schaefer[81], D. Scott[17], G. F. Smoot[23,67,3], J.-L. Starck[64,12], D. Sutton[55,62], J.-F. Sygnet[51,80], J. A. Tauber[37], L. Terenzi[43], L. Toffolatti[15], M. Tomasi[28,44], M. Tristram[66], M. Türler[46], L. Valenziano[43], P. Vielva[58], F. Villa[43], N. Vittorio[31], L. A. Wade[60], B. D. Wandelt[51,80,25], J. Weller[83], S. D. M. White[68], M. White[23], D. Yvon[12], A. Zacchei[42], and A. Zonca[24]

(Affiliations can be found after the references)

ABSTRACT

We present first results on PLCK G266.6−27.3, a galaxy cluster candidate detected at a signal-to-noise ratio of 5 in the *Planck* All Sky survey. An *XMM-Newton* validation observation has allowed us to confirm that the candidate is a bona fide galaxy cluster. With these X-ray data we measure an accurate redshift, $z = 0.94 \pm 0.02$, and estimate the cluster mass to be $M_{500} = (7.8 \pm 0.8) \times 10^{14}$ $M_\odot$. PLCK G266.6−27.3 is an exceptional system: its luminosity of $L_X[0.5-2.0 \text{ keV}] = (1.4 \pm 0.05) \times 10^{45}$ erg s^{-1} equals that of the two most luminous known clusters in the $z > 0.5$ universe, and it is one of the most massive clusters at $z \sim 1$. Moreover, unlike the majority of high-redshift clusters, PLCK G266.6−27.3 appears to be highly relaxed. This observation confirms *Planck*'s capability of detecting high-redshift, high-mass clusters, and opens the way to the systematic study of population evolution in the exponential tail of the mass function.

Key words. cosmology: observations – galaxies: clusters: general – galaxies: clusters: intracluster medium – X-rays: galaxies: clusters – cosmic background radiation

1. Introduction

Very massive clusters above redshift $z \sim 1$, when the Universe was at half the present age, are predicted to be very rare.

⋆ Corresponding author: M. Arnaud,
e-mail: monique.arnaud@cea.fr

They potentially provide a sensitive probe to constrain deviations from the standard ΛCDM paradigm (e.g. Mortonson et al. 2011); e.g., owing to non-Gaussian perturbations, non-standard quintessence models or modified gravity models (see Allen et al. 2011, for a review). They are also ideal targets for studying key aspects of the gravitational physics that drives cluster formation,

including measurement of the evolution of the mass concentration. For these reasons, the scientific community has, over the past two decades, put strong effort into the discovery and characterisation of these objects.

Until recently it was possible to identify clusters of galaxies only via optical/infrared or X-ray surveys. Indeed, the most distant clusters presently known have all been detected with these techniques, e.g., the IR-selected cluster CL J1449+0856 at $z = 2.07$ (Gobat et al. 2011) and the X-ray selected system XMMU J105324.7+572348 at $z = 1.75$ (Henry et al. 2010). For both of these objects, extended X-ray emission has been detected with *XMM-Newton*, confirming their status as fully established galaxy clusters; however, their total masses are more typical of systems in the poor cluster or group regime ($\lesssim 10^{14}\ M_\odot$). Until recently, the most massive cluster known in the $z \gtrsim 1$ universe was XMMU J2235.3−2557 at $z = 1.39$, discovered in the *XMM-Newton* Distant Cluster Project (XDCP) based on serendipitous cluster searches in *XMM-Newton* observations (Mullis et al. 2005). For this system, Jee et al. (2009) estimate a mass of $M_{200} = (7.3 \pm 1.3) \times 10^{14}\ M_\odot$ from a weak lensing analysis.

However, clusters are also detectable through the Sunyaev-Zeldovich (SZ) effect (Sunyaev & Zeldovich 1972), the spectral distortion of the cosmic microwave background (CMB) generated via inverse Compton scattering of CMB photons by the hot electrons in the intra-cluster medium. Crucially, the total SZ signal is expected to be closely related to the cluster mass (e.g. da Silva et al. 2004), and its brightness insensitive to redshift dimming. As a result, SZ surveys can potentially provide unbiased cluster samples that are as close as possible to being mass-selected[1]. They offer an ideal way to identify massive, high-redshift clusters. One recent illustration is the detection of SPT-CL J2106−5844 at $z = 1.13$ by the South Pole Telescope (SPT) survey (Foley et al. 2011). With an estimated mass of $M_{200} = (1.27 \pm 0.21) \times 10^{15}\ M_\odot$, SPT-CL J2106−5844 is nearly twice as massive as XMMU J2235.3−2557.

The *Planck*[2] satellite has been surveying the sky in the microwave band since August 2009 (Planck Collaboration 2011a) with a good (band-dependent) spatial resolution of 5 arcmin (Mennella et al. 2011; Planck HFI Core Team 2011a). Compared to other SZ experiments such as ACT (Marriage et al. 2011) or SPT (Carlstrom et al. 2011), *Planck* brings unique nine-band coverage from 30 to 857 GHz and, most crucially, an exceptionally large survey volume. *Planck* is the first all-sky survey capable of blindly detecting clusters (i.e., not guided in the search by prior observations), since the ROSAT All-Sky Survey (RASS) in the X-ray domain. This coverage allows detection of the rarest clusters, the most massive objects lying in the exponential tail of the mass function.

Planck Collaboration (2011d) recently published the early SZ (ESZ) sample, the first sample of galaxy clusters detected blindly in the all-sky maps from the first ten months of the *Planck* survey. The properties of this first sample already show that *Planck* is detecting previously unknown, massive clusters that do not appear in RASS or in other smaller area SZ surveys

(Planck Collaboration 2011e). The ESZ comprises high signal-to-noise ratio ($S/N > 6$) *Planck* SZ sources up to $z = 0.5$. We report here on an SZ source that was blindly identified at $S/N \sim 5$ in the *Planck* all-sky survey, and recent *XMM-Newton* validation observations confirm it is a massive cluster at $z \sim 1$.

In this paper, we adopt a ΛCDM cosmology with $H_0 = 70\ \mathrm{km\,s^-\ Mpc}$, $\Omega_M = 0.3$, and $\Omega_\Lambda = 0.7$. The factor $E(z) = \sqrt{\Omega_M (1+z)^3 + \Omega_\Lambda}$ is the ratio of the Hubble constant at redshift z to its present-day value. The quantities M_δ and R_δ are the total mass and radius corresponding to a total density contrast δ, as compared to $\rho_c(z)$, the critical density of the Universe at the cluster redshift; $M_\delta = (4\pi/3)\,\delta\,\rho_c(z)\,R_\delta^3$. The SZ flux is characterised by Y_{500}, where $Y_{500}\,D_A^2$ is the spherically integrated Compton parameter within R_{500} (corresponding to $\delta = 500$), and D_A is the angular-diameter distance to the cluster.

2. *Planck* detection

The blind search for clusters in *Planck* data relies on a multi-matched filter (MMF) approach (Melin et al. 2006). Candidates then undergo a validation process, including internal quality checks and cross-correlation with ancillary data and catalogues, as described in Planck Collaboration (2011d). This process produces a list of new *Planck* SZ cluster candidates above a given S/N threshold that require follow-up for confirmation. The *XMM-Newton* follow-up for validation, undertaken in Director's Discretionary Time via an agreement between the *XMM-Newton* and *Planck* Project Scientists, plays a central role in this confirmation procedure. It consists of snapshot exposures (~10 ks), sufficient for unambiguous discrimination between clusters and false candidates (Planck Collaboration 2011e). The results of the first two runs (completed in September 2010) are reported by Planck Collaboration (2011d,e).

The *XMM-Newton* validation programme is continuing to explore lower S/N and detection quality criteria. PLCK G266.6−27.3, detected at $S/N = 5.03$, was observed in the framework of the third run of the *XMM-Newton* validation programme, for which the analysis is on-going. This run comprises a total of 11 candidates detected at $4.5 < S/N < 5.3$ from the same *Planck* HFI maps used for the construction the ESZ sample. The 11 candidates were sent for scheduling in November 2010 and the observations were performed between 22 December 2010 and 16 May 2011. Interestingly, PLCK G266.6−27.3 has been independently detected in the SPT survey. Its *Planck* position ($6^{\mathrm{h}}16^{\mathrm{m}}6\overset{.}{.}6$, $−57°47′29″$) is consistent with that of SPT-CL J0615-5746 (Williamson et al. 2011, published on `arXiv.org` in January 2011, with a photometric redshift of $z_{\mathrm{phot}} = 1 \pm 0.1$).

3. *XMM-Newton* validation

3.1. Observation and data reduction

PLCK G266.6−27.3 was observed with the *XMM-Newton* EPIC instrument (Turner et al. 2001; Strüder et al. 2001), using the thin filters and the extended full frame mode for the "pn-CCD" camera. The data analysis and validation procedure is described in Planck Collaboration (2011e). Calibrated event lists were produced with v11.0 of the *XMM-Newton* Science Analysis System. Data that are affected by periods of high background due to soft proton flares were omitted from the analysis, and the remaining data were PATTERN-selected and corrected for vignetting, as described in Pratt et al. (2007). Bright point sources were excised

---

[1] In practice, the mass threshold detectable by *Planck* increases with redshift. The total SZ signal is not resolved by *Planck* at high z and it decreases with z due to the decreasing angular size of the object.

[2] *Planck* (http://www.esa.int/Planck) is a project of the European Space Agency (ESA) with instruments provided by two scientific consortia funded by ESA member states (in particular the lead countries: France and Italy) with contributions from NASA (USA), and telescope reflectors provided in a collaboration between ESA and a scientific consortium led and funded by Denmark.
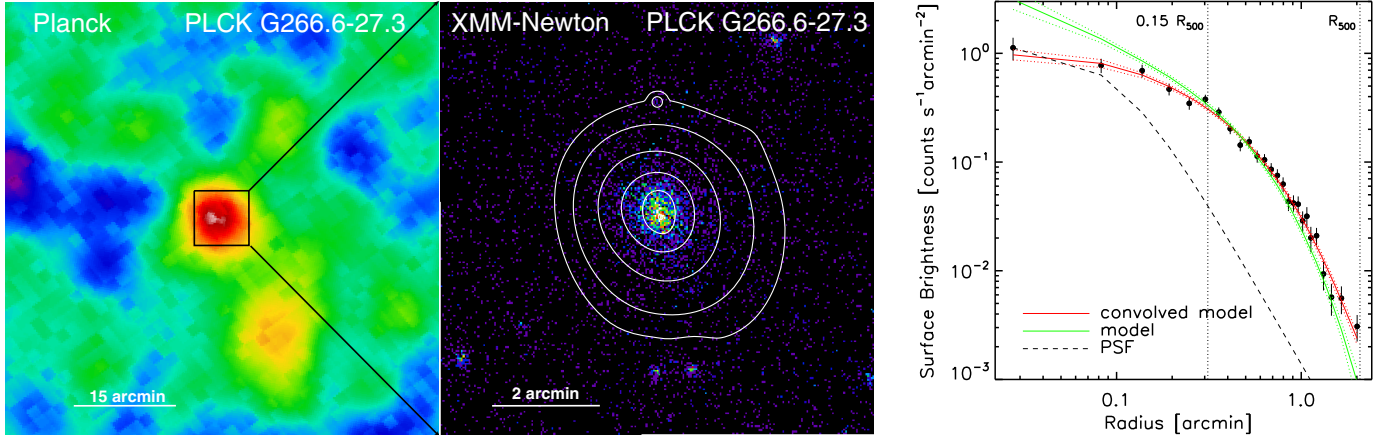
Fig. 1. *Left panel*: *Planck* Y_{SZ} map of PLCK G266.6−27.3 obtained with the modified internal linear combination algorithm (MILCA; Hurier et al. 2010) with a spatial resolution of 10′. *Middle panel*: *XMM-Newton* exposure-corrected count rate image of the region indicated by the black box in *the left panel*. It is obtained using data from the EMOS1&2 and EPN camera in the [0.3−2.0] keV energy band. The contours of the *XMM-Newton* image after wavelet filtering are overlaid in white. *Right panel*: corresponding *XMM-Newton* surface brightness profile. The green line indicates the best-fitting β-model with a cusp (see text); the red line is this model convolved with the point spread function (PSF) of *XMM-Newton*, and the dashed line is the on-axis PSF of *XMM-Newton*, normalised to the central intensity. The source is clearly significantly extended.

from the data. Background treatment is described in Pratt et al. (2010). In the spectroscopic analysis, the cluster component was modelled with an absorbed thermal emission model (mekal) with a hydrogen column density fixed at the 21-cm value of Dickey & Lockman (1990).

The observation, OBSID = 0658200101, was affected by soft proton flares. The net exposure time after flare cleaning is only 2.4 ks for the pn-CCD camera, with a particle background 30% higher than nominal. The MOS camera data are less affected with a clean time of ∼12 ks and a background excess about two times lower. We undertook a conservative approach to analysing spectroscopic data, since they are the most sensitive to the background estimate. We first fitted the data from the three cameras simultaneously, then fitted only the MOS cameras. The uncertainties in the physical quantities below reflect the difference in best-fitting values between the two analyses and their errors.

3.2. Confirmation and z estimate

In Fig. 1 we show the vignetting-corrected count rate image of the cluster in the [0.3−2.0] keV band. An extended X-ray source is clearly coincident with PLCK G266.6−27.3. Its total EPIC count rate in the [0.3−2.0] keV band is (0.52 ± 0.02) count/s within 2.3′, the maximum radius of detection. The offset between the X-ray cluster centre, defined as the emission peak at $6^h15^m51\overset{s}{.}7$, $-57°46'52\overset{''}{.}8$, and the *Planck* blind position is 2′.07, consistent with the position reconstruction uncertainty, driven by the *Planck* spatial resolution and the source S/N (Planck Collaboration 2011d). The extended nature of the source is confirmed by comparing the surface brightness profile with the *XMM-Newton* point spread function (PSF) (Fig. 1, right panel). A typical (PSF-convolved) cluster surface brightness model consisting of a β-model with a central cusp (Eq. (2) in Pratt & Arnaud 2002) provides a good fit to the data and further supports the extended nature of the source (Fig. 1).

We extracted a spectrum within a circular region corresponding to the maximum significance of the X-ray detection ($\theta \lesssim 1'.5$). The iron K line complex is clearly detected (Fig. 2). Its significance is 3.6σ, estimated from a fit of the spectrum
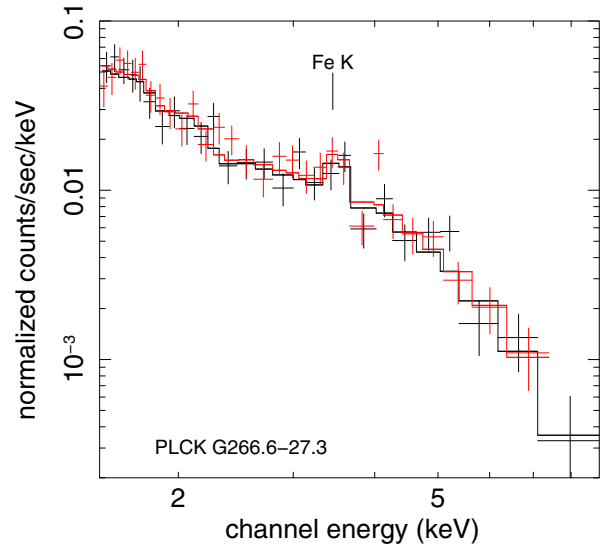

Fig. 2. *XMM-Newton* EMOS1 (black) and EMOS2 (red) spectra extracted from a circular region of 1′.5 in radius and centred in the cluster X-ray peak. Only the data points above 2 keV are shown for clarity, but data down to 0.3 keV are used in the spectral fitting. The line is the thermal model for the best-fitting redshift, $z = 0.94 \pm 0.02$. The position of the redshifted Fe K line is marked.

in the [2−6] keV band with a continuum plus a Gaussian line model. Since the centroid of the line complex depends on the temperature, the redshift is determined from a thermal model fit to the full spectrum, as described in detail in Planck Collaboration (2011e). This yields a precise redshift estimate of $z = 0.94 \pm 0.02$.

4. Physical cluster properties

4.1. An exceptionally luminous and massive cluster

We derived the deprojected, PSF-corrected gas density profile from the surface brightness profile, using the non-parametric method described in Croston et al. (2006). Global

Table 1. Physical properties of PLCK G266.6−27.3 derived from *XMM-Newton* data.

Parameter	Value
z	0.94 ± 0.02
Abundance	0.44 ± 0.17 solar
R_{500}	0.98 ± 0.03 Mpc
M_{500}	$7.8^{+0.8}_{-0.7} \times 10^{14}$ M$_\odot$
Y_X	$1.10^{+0.20}_{-0.17} \times 10^{15}$ M$_\odot$ keV
T_X	$10.5^{+1.6}_{-1.4}$ keV
$T(<R_{500})$	$11.4^{+1.4}_{-1.2}$ keV
$L_{500}([0.5–2.0]$ keV$)$	$14.2 \pm 0.5 \times 10^{44}$ erg s^{-1}
$L_{500}([0.1–2.4]$ keV$)$	$22.7 \pm 0.8 \times 10^{44}$ erg s^{-1}

Notes. The $M_{500} - Y_X$ relation with self-similar evolution is used to estimate R_{500} (see Sect. 4).

Table 2. SZ flux derived from *Planck* data with the reference value indicated in boldface.

Method	Definition	Value $(10^{-4}$ arcmin$^2)$	θ_{500} (arcmin)
MMF blind	Y_{500}	5.6 ± 3.0	3.3 ± 2.8
PWS blind	Y_{500}	6.5 ± 1.8	3.9 ± 1.6
MMF X-ray prior	Y_{500}	**4.1 ± 0.9**	fixed
PWS X-ray prior	Y_{500}	5.3 ± 0.9	fixed
MILCA	Y_{tot}	5.9 ± 1.0	. . .

Notes. Uncertainties on the blind values take into account the size uncertainty.

cluster parameters were then estimated self-consistently within R_{500} via iteration about the $M_{500} - Y_X$ relation of Arnaud et al. (2010), assuming standard evolution, $E(z)^{2/5} M_{500} = 10^{14.567\pm0.010} \left[\frac{Y_X}{2\times10^{14}\ M_\odot\ \mathrm{keV}} \right]^{0.561\pm0.018}$ $M_\odot$. The quantity Y_X, introduced by Kravtsov et al. (2006), is defined as the product of $M_{g,500}$, the gas mass within R_{500}, and T_X. T_X is the spectroscopic temperature measured in the $[0.15−0.75]\,R_{500}$ aperture. In addition, L_{500}, the X-ray luminosity inside R_{500}, was calculated as described in Pratt et al. (2009). All resulting X-ray properties, including iron abundance, are summarised in Table 1.

PLCK G266.6−27.3 is an exceptionally luminous system. Its $[0.1−2.4]$ keV band luminosity of $(22.7 \pm 0.8) \times 10^{44}$ erg s^{-1} is equal to that of the fifth most luminous object in the MCXC compilation of Piffaretti et al. (2011), MACS J0717.5+3745 at $z = 0.55$, discovered in the RASS by Edge et al. (2003). Moreover, its $[0.5−2.0]$ keV band luminosity is consistent with that of SPT-CL J2106−5844, the most luminous cluster known beyond $z = 1$ (Foley et al. 2011). Collectively, these three clusters are the most luminous systems at $z > 0.5$. They are only 40% fainter than RXJ 1347.5-1145, the most X-ray luminous cluster known in the Universe (Piffaretti et al. 2011).

Consistent with expectations for high-redshift *Planck*-detected clusters, we find that this cluster is extremely hot, $T_X \sim$ 11 keV, and massive, with a mass of $M_{500} = 7.8^{+0.8}_{-0.7} \times 10^{14}$ $M_\odot$. Our mass estimate is consistent with the less precise value, $M_{500} = 8 \pm 2$ (statistical) ± 1.9 (systematic) $\times 10^{14}$ $M_\odot$, which is derived by Williamson et al. (2011) using the relation between SPT S/N and mass. Comparison of the masses of high-redshift systems is not trivial, because the estimation strongly depends on method, e.g. which mass proxy is used and at what reference radius the mass is measured. On the basis of the published mass estimates, PLCK G266.6−27.3 would appear to be the most massive cluster at $z \sim 1$. Using the same factor to convert M_{500} to M_{200} as Foley et al. (2011), we obtain $M_{200} = 15.5^{+1.5}_{-1.4} \times 10^{14}$ $M_\odot$, to be compared to $M_{200} = (12.7 \pm 2.1)^{3} \times 10^{14}$ $M_\odot$ for SPT-CL J2106-5844. However, the last value was derived by combining X-ray and SZ data. A more direct comparison of M_{500} values estimated from the $M_{500} - Y_X$ relation indicates that they are identical within their uncertainties: $M_{500} = (7.8 \pm 0.8) \times 10^{14}$ $M_\odot$ for PLCK G266.6−27.3 and $M_{500} = (9.3 \pm 2.0) \times 10^{14}$ $M_\odot$ for SPT-CL J2106−5844.

4.2. Y_{500} Compton parameter versus Y_X

The MMF blind detection was performed using the universal pressure profile of Arnaud et al. (2010) as a spatial template, leaving the position, characteristic size, θ_{500}, and SZ flux, Y_{500}, as free parameters. The resulting flux, $Y_{500} = (5.6 \pm 3.0) \times 10^{-4}$ arcmin^2, is consistent with the value, $Y_{500}^X = 6.4^{+1.2}_{-1.0} \times 10^{-4}$ arcmin^2, expected from the measured value of Y_X using the scaling relation derived from the universal pressure profile (Arnaud et al. 2010, Eq. (19)). The cluster size, comparable to *Planck*'s spatial resolution, is poorly constrained, $\theta_{500} = 3'.3 \pm 2'.8$. As discussed in Planck Collaboration (2011d), the uncertainty on the blind Y_{500} value is then large because of the flux-size degeneracy, where an overestimate of the cluster size induces an overestimate of the SZ signal. The SZ photometry can be improved by using the more precise *XMM-Newton* position and size in the flux extraction. The Y_{500} value obtained using these X-ray priors, $Y_{500} = (4.1 \pm 0.9) \times 10^{-4}$ arcmin^2, is lower than the value expected from the X-ray data at the 1.7σ significance level.

To check the robustness of the Y_{500} estimate, we compared the MMF value with the one derived from the PowellSnakes (PWS; Carvalho et al. 2009, and in prep.) algorithm and the modified internal linear combination algorithm (MILCA; Hurier et al. 2010). The values are given in Table 2. PWS is a blind detection algorithm that assumes the same profile shape as MMF, but is based on a Bayesian statistical approach, as fully described in Carvalho et al. (2009). MMF and PWS give consistent results, the difference between MMF and PWS Y_{500} values being about 1.3 times the respective 1σ uncertainties. MILCA is a component separation method that allows reconstruction of the SZ map around the cluster from an optimised linear combination of *Planck* HFI maps. In contrast to the MMF and PWS methods, the SZ flux derived from MILCA is obtained from aperture photometry, i.e., with no assumptions on SZ profile shape or size. Assuming a typical conversion factor of 2/3 based on the universal profile to convert the total Y_{tot} MILCA measurement to Y_{500}, the MMF and MILCA estimates are in excellent agreement.

Several factors may affect the X-ray and SZ flux measurements and bring them out of accord. We have checked for possible AGN contamination that could lower the Y_{500} value using the NVSS (at 1.4 GHz, Condon et al. 1998) and SUMSS (at 0.84 GHz, Bock et al. 1999) catalogues, but no bright radio sources are found in the cluster vicinity. The closest radio source with significant flux density is at $12'.6$ away. The source has a 1 GHz flux density of 0.46 Jy. We also find no evidence of radio contamination in the low-frequency *Planck* bands. On the other hand, the Y_X measurement may also be increased by AGN contamination, from cluster members or foreground/background

---

[3] The error includes an extra ∼15% error accounting for uncertainties in the scaling relations.

galaxies. Point source contamination is difficult to estimate owing to the *XMM-Newton* PSF. So, we estimate a maximum contribution to the X-ray luminosity from a central active galaxy of ≲20%, assuming a point source model normalised to the central value of the X-ray surface brightness. The contribution to the gas mass, hence to Y_X, would be less, provided that the source is not hard enough to significantly affect T_X. Nevertheless, only high-resolution X-ray imaging (e.g., from *Chandra*) can definitively establish whether X-ray AGNs at the cluster location affect our luminosity or mass measurement. A departure from the universal pressure profile would change the Y_{500}/Y_X ratio. The density profile shown below does not show any indication of this effect; however, deep spatially resolved *XMM-Newton* and *Chandra* spectroscopic observations are needed to derive the radial pressure gradient from the core to R_{500}. A final interesting possibility is that gas clumping could affect the Y_X measurements. A combination of X-ray and higher resolution SZ observations is required to assess this point.

4.3. Dynamical state and self-similarity of shape up to high z

The available information indicates that PLCK G266.6−27.3 may be particularly dynamically relaxed. The cluster image (Fig. 1, middle panel) does not show any sign of disturbance: the surface brightness is quite regular and quasi-azimuthally symmetric within R_{500}. The offset between the X-ray surface brightness peak and the cluster brightest galaxy (Williamson et al. 2011, Fig. 19) is less than 5″.

To further examine the dynamical state of the cluster, in Fig. 3 we compare its scaled density profile to those of clusters in the local representative X-ray-selected sample REXCESS (Böhringer et al. 2007; Croston et al. 2008). The radii are scaled by R_{500} and the density by the mean within R_{500}. As extensively discussed by Pratt et al. (2009) and Arnaud et al. (2010), morphologically disturbed (i.e., merging) systems have systematically shallower density profiles than more relaxed cool core objects. This is illustrated in Fig. 3, where we indicate the scaled density profiles of the more relaxed cool core and the dynamically active merging clusters. The scaled density profile of PLCK G266.6−27.3 lies between the two classes, but with an indication of being closer to the relaxed rather than the merging systems. It is thus possible that PLCK G266.6−27.3 is a cool core object at $z \sim 1$. Such objects are expected to be rare (e.g., Vikhlinin et al. 2007; Santos et al. 2010), and no cluster at this redshift has yet been found to contain a resolved central temperature drop that would confirm the presence of a cool core. A deep exposure at *Chandra* spatial resolution is needed to check this hypothesis.

It is worth emphasising the similarity beyond the core of the density profile of this cluster with respect to REXCESS systems. This is the first piece of evidence for a similarity of shape up to redshifts as high as $z \sim 1$.

5. Conclusion

PLCK G266.6−27.3 is the first blindly discovered *Planck* cluster of galaxies at $z \sim 1$. It has been confirmed by *XMM-Newton* in the framework of the on-going validation DDT observations. *XMM-Newton* data allowed us to measure the redshift with high accuracy ($z = 0.94 \pm 0.02$) and estimate the cluster mass to be $M_{500} = (7.8 \pm 0.8) \times 10^{14} \, M_\odot$. This *XMM-Newton* confirmation and redshift estimate is a clear demonstration of the capability of *Planck* for detecting high-z, high-mass clusters.
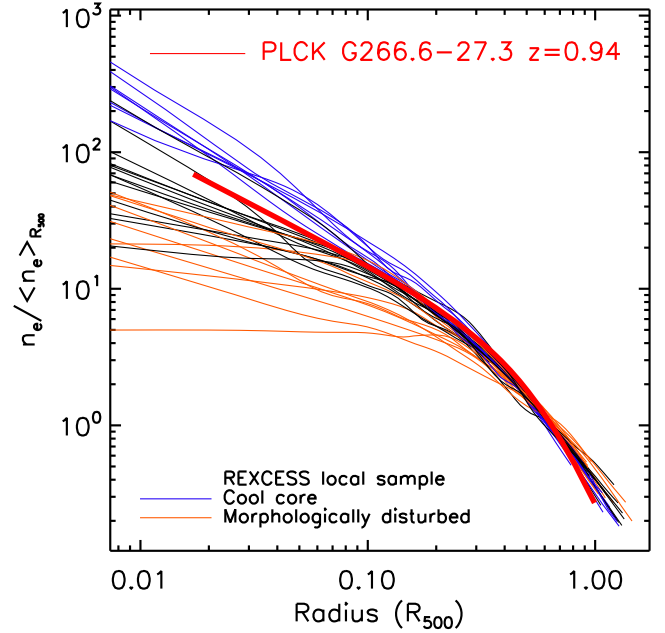

Fig. 3. Scaled density profiles of the REXCESS local cluster sample (Böhringer et al. 2007; Croston et al. 2008). The blue lines show the profiles for the cool core systems, and the orange lines the density profiles of the morphologically disturbed systems. The density profile of PLCK G266.6−27.3 is shown with a thick red line.

PLCK G266.6−27.3 is an exceptional system, both in terms of its luminosity and its estimated mass. Furthermore, unlike other high-redshift clusters, it is likely to be a relaxed system, potentially allowing accurate hydrostatic mass measurements. It is thus a perfect target for deep multi-wavelength follow-up to address such important cosmological issues as the evolution of dark matter profiles, the evolution of the mass-Y_{SZ} relation, gas clumping, and the bias between X-ray and lensing mass estimates at such high redshift.

References

Allen, S. W., Evrard, A. E., & Mantz, A. B. 2011, ARA&A, 49, 409
Arnaud, M., Pratt, G. W., Piffaretti, R., et al. 2010, A&A, 517, A92
Bock, D., Large, M. I., & Sadler, E. M. 1999, AJ, 117, 1578
Böhringer, H., Schuecker, P., Pratt, G. W., et al. 2007, A&A, 469, 363
Carlstrom, J. E., Ade, P. A. R., Aird, K. A., et al. 2011, PASP, 123, 568

Carvalho, P., Rocha, G., & Hobson, M. P. 2009, MNRAS, 393, 681
Condon, J. J., Cotton, W. D., Greisen, E. W., et al. 1998, AJ, 115, 1693
Croston, J. H., Arnaud, M., Pointecouteau, E., & Pratt, G. W. 2006, A&A, 459, 1007
Croston, J. H., Pratt, G. W., Böhringer, H., et al. 2008, A&A, 487, 431
da Silva, A. C., Kay, S. T., Liddle, A. R., & Thomas, P. A. 2004, MNRAS, 348, 1401
Dickey, J. M., & Lockman, F. J. 1990, ARA&A, 28, 215
Edge, A. C., Ebeling, H., Bremer, M., et al. 2003, MNRAS, 339, 913
Foley, R. J., Andersson, K., Bazin, G., et al. 2011, ApJ, 731, 86
Gobat, R., Daddi, E., Onodera, M., et al. 2011, A&A, 526, A133
Henry, J. P., Salvato, M., Finoguenov, A., et al. 2010, ApJ, 725, 615
Hurier, G., Hildebrandt, S. R., & Macias-Perez, J. F. 2010, unpublished [arXiv:1007.1149]
Jee, M. J., Rosati, P., Ford, H. C., et al. 2009, ApJ, 704, 672
Kravtsov, A. V., Vikhlinin, A., & Nagai, D. 2006, ApJ, 650, 128
Marriage, T. A., Baptiste Juin, J., Lin, Y., et al. 2011, ApJ, 731, 100
Melin, J., Bartlett, J. G., & Delabrouille, J. 2006, A&A, 459, 341
Mennella, A., Bersanelli, M., Butler, R. C., et al. 2011, A&A, 536, A3
Mortonson, M. J., Hu, W., & Huterer, D. 2011, Phys. Rev. D, 83, 023015
Mullis, C. R., Rosati, P., Lamer, G., et al. 2005, ApJ, 623, L85
Piffaretti, R., Arnaud, M., Pratt, G. W., Pointecouteau, E., & Melin, J. 2011, A&A, 534, A109
Planck Collaboration 2011a, A&A, 536, A1
Planck Collaboration 2011b, A&A, 536, A2
Planck Collaboration 2011c, A&A, 536, A7
Planck Collaboration 2011d, A&A, 536, A8
Planck Collaboration 2011e, A&A, 536, A9
Planck Collaboration 2011f, A&A, 536, A10
Planck Collaboration 2011g, A&A, 536, A11
Planck Collaboration 2011h, A&A, 536, A12
Planck Collaboration 2011i, A&A, 536, A13
Planck Collaboration 2011j, A&A, 536, A14
Planck Collaboration 2011k, A&A, 536, A15
Planck Collaboration 2011l, A&A, 536, A16
Planck Collaboration 2011m, A&A, 536, A17
Planck Collaboration 2011n, A&A, 536, A18
Planck Collaboration 2011o, A&A, 536, A19
Planck Collaboration 2011p, A&A, 536, A20
Planck Collaboration 2011q, A&A, 536, A21
Planck Collaboration 2011r, A&A, 536, A22
Planck Collaboration 2011s, A&A, 536, A23
Planck Collaboration 2011t, A&A, 536, A24
Planck Collaboration 2011u, A&A, 536, A25
Planck Collaboration 2011v, The Explanatory Supplement to the Planck Early Release Compact Source Catalogue (ESA)
Planck Collaboration 2011w, A&A, 536, A26
Planck HFI Core Team 2011a, A&A, 536, A4
Planck HFI Core Team 2011b, A&A, 536, A6
Pratt, G. W., & Arnaud, M. 2002, A&A, 394, 375
Pratt, G. W., Böhringer, H., Croston, J. H., et al. 2007, A&A, 461, 71
Pratt, G. W., Croston, J. H., Arnaud, M., & Böhringer, H. 2009, A&A, 498, 361
Pratt, G. W., Arnaud, M., Piffaretti, R., et al. 2010, A&A, 511, A85
Santos, J. S., Tozzi, P., Rosati, P., & Böhringer, H. 2010, A&A, 521, A64
Strüder, L., Briel, U., Dennerl, K., et al. 2001, A&A, 365, L18
Sunyaev, R. A., & Zeldovich, Y. B. 1972, Comm. Astrophys. Space Phys., 4, 173
Turner, M. J. L., Abbey, A., Arnaud, M., et al. 2001, A&A, 365, L27
Vikhlinin, A., Burenin, R., Forman, W. R., et al. 2007, in Heating versus Cooling in Galaxies and Clusters of Galaxies, ed. H. Böhringer, G. W. Pratt, A. Finoguenov, & P. Schuecker (Berlin, Heidelberg: Springer-Verlag), 48
Williamson, R., Benson, B. A., High, F. W., et al. 2011, ApJ, 738, 139
Zacchei, A., Maino, D., Baccigalupi, C., et al. 2011, A&A, 536, A5

[1] Aalto University Metsähovi Radio Observatory, Metsähovintie 114, 02540 Kylmälä, Finland
[2] Agenzia Spaziale Italiana Science Data Center, c/o ESRIN, via Galileo Galilei, Frascati, Italy
[3] Astroparticule et Cosmologie, CNRS (UMR7164), Université Denis Diderot Paris 7, Bâtiment Condorcet, 10 rue A. Domon et Léonie Duquet, Paris, France
[4] Astrophysics Group, Cavendish Laboratory, University of Cambridge, J J Thomson Avenue, Cambridge CB3 0HE, UK
[5] Atacama Large Millimeter/submillimeter Array, ALMA Santiago Central Offices, Alonso de Cordova 3107, Vitacura, Casilla 763 0355, Santiago, Chile
[6] CITA, University of Toronto, 60 St. George St., Toronto, ON M5S 3H8, Canada
[7] CNRS, IRAP, 9 Av. colonel Roche, BP 44346, 31028 Toulouse Cedex 4, France
[8] California Institute of Technology, Pasadena, California, USA
[9] Centre of Mathematics for Applications, University of Oslo, Blindern, Oslo, Norway
[10] Centro de Astrofísica, Universidade do Porto, Rua das Estrelas, 4150-762 Porto, Portugal
[11] Centro de Estudios de Física del Cosmos de Aragón (CEFCA), Plaza San Juan, 1, planta 2, 44001 Teruel, Spain
[12] DSM/Irfu/SPP, CEA-Saclay, 91191 Gif-sur-Yvette Cedex, France
[13] DTU Space, National Space Institute, Juliane Mariesvej 30, Copenhagen, Denmark
[14] Departamento de Física Fundamental, Facultad de Ciencias, Universidad de Salamanca, 37008 Salamanca, Spain
[15] Departamento de Física, Universidad de Oviedo, Avda. Calvo Sotelo s/n, Oviedo, Spain
[16] Department of Astronomy and Astrophysics, University of Toronto, 50 Saint George Street, Toronto, Ontario, Canada
[17] Department of Physics & Astronomy, University of British Columbia, 6224 Agricultural Road, Vancouver, British Columbia, Canada
[18] Department of Physics and Astronomy, University of Southern California, Los Angeles, California, USA
[19] Department of Physics and Astronomy, University of Sussex, Brighton BN1 9QH, UK
[20] Department of Physics, Gustaf Hällströmin katu 2a, University of Helsinki, Helsinki, Finland
[21] Department of Physics, Princeton University, Princeton, New Jersey, USA
[22] Department of Physics, Purdue University, 525 Northwestern Avenue, West Lafayette, Indiana, USA
[23] Department of Physics, University of California, Berkeley, California, USA
[24] Department of Physics, University of California, Santa Barbara, California, USA
[25] Department of Physics, University of Illinois at Urbana-Champaign, 1110 West Green Street, Urbana, Illinois, USA
[26] Dipartimento di Fisica G. Galilei, Università degli Studi di Padova, via Marzolo 8, 35131 Padova, Italy
[27] Dipartimento di Fisica, Università La Sapienza, P.le A. Moro 2, Roma, Italy
[28] Dipartimento di Fisica, Università degli Studi di Milano, via Celoria 16, Milano, Italy
[29] Dipartimento di Fisica, Università degli Studi di Trieste, via A. Valerio 2, Trieste, Italy
[30] Dipartimento di Fisica, Università di Ferrara, via Saragat 1, 44122 Ferrara, Italy
[31] Dipartimento di Fisica, Università di Roma Tor Vergata, via della Ricerca Scientifica 1, Roma, Italy
[32] Discovery Center, Niels Bohr Institute, Blegdamsvej 17, Copenhagen, Denmark
[33] Dpto. Astrofísica, Universidad de La Laguna (ULL), 38206 La Laguna, Tenerife, Spain
[34] European Southern Observatory, ESO Vitacura, Alonso de Cordova 3107, Vitacura, Casilla 19001, Santiago, Chile
[35] European Space Agency, ESAC, Camino bajo del Castillo s/n, Urbanización Villafranca del Castillo, Villanueva de la Cañada, Madrid, Spain
[36] European Space Agency, ESAC, Planck Science Office, Camino bajo del Castillo s/n, Urbanización Villafranca del Castillo, Villanueva de la Cañada, Madrid, Spain
[37] European Space Agency, ESTEC, Keplerlaan 1, 2201 AZ Noordwijk, The Netherlands
[38] Finnish Centre for Astronomy with ESO (FINCA), University of Turku, Väisäläntie 20, 21500, Piikkiö, Finland
[39] Helsinki Institute of Physics, Gustaf Hällströmin katu 2, University of Helsinki, Helsinki, Finland

[40] INAF - Osservatorio Astronomico di Padova, Vicolo dell'Osservatorio 5, Padova, Italy

[41] INAF - Osservatorio Astronomico di Roma, via di Frascati 33, Monte Porzio Catone, Italy

[42] INAF - Osservatorio Astronomico di Trieste, via G.B. Tiepolo 11, Trieste, Italy

[43] INAF/IASF Bologna, via Gobetti 101, Bologna, Italy

[44] INAF/IASF Milano, via E. Bassini 15, Milano, Italy

[45] IPAG (Institut de Planétologie et d'Astrophysique de Grenoble), Université Joseph Fourier, Grenoble 1/CNRS-INSU, UMR 5274, Grenoble, 38041, France

[46] ISDC Data Centre for Astrophysics, University of Geneva, ch. d'Ecogia 16, Versoix, Switzerland

[47] Imperial College London, Astrophysics group, Blackett Laboratory, Prince Consort Road, London SW7 2AZ, UK

[48] Infrared Processing and Analysis Center, California Institute of Technology, Pasadena, CA 91125, USA

[49] Institut Néel, CNRS, Université Joseph Fourier Grenoble I, 25 rue des Martyrs, Grenoble, France

[50] Institut d'Astrophysique Spatiale, CNRS (UMR8617) Université Paris-Sud 11, Bâtiment 121, Orsay, France

[51] Institut d'Astrophysique de Paris, CNRS (UMR7095), 98bis boulevard Arago, 75014, Paris, France

[52] Institut de Ciències de l'Espai, CSIC/IEEC, Facultat de Ciències, Campus UAB, Torre C5 par-2, Bellaterra 08193, Spain

[53] Institute for Space Sciences, Bucharest-Magurale, Romania

[54] Institute of Astronomy and Astrophysics, Academia Sinica, Taipei, Taiwan

[55] Institute of Astronomy, University of Cambridge, Madingley Road, Cambridge CB3 0HA, UK

[56] Institute of Theoretical Astrophysics, University of Oslo, Blindern, Oslo, Norway

[57] Instituto de Astrofísica de Canarias, C/Vía Láctea s/n, La Laguna, Tenerife, Spain

[58] Instituto de Física de Cantabria (CSIC-Universidad de Cantabria), Avda. de los Castros s/n, Santander, Spain

[59] Istituto di Fisica del Plasma, CNR-ENEA-EURATOM Association, via R. Cozzi 53, Milano, Italy

[60] Jet Propulsion Laboratory, California Institute of Technology, 4800 Oak Grove Drive, Pasadena, California, USA

[61] Jodrell Bank Centre for Astrophysics, Alan Turing Building, School of Physics and Astronomy, The University of Manchester, Oxford Road, Manchester M13 9PL, UK

[62] Kavli Institute for Cosmology Cambridge, Madingley Road, Cambridge CB3 0HA, UK

[63] LERMA, CNRS, Observatoire de Paris, 61 avenue de l'Observatoire, Paris, France

[64] Laboratoire AIM, IRFU/Service d'Astrophysique – CEA/DSM – CNRS – Université Paris Diderot, Bât. 709, CEA-Saclay, 91191 Gif-sur-Yvette Cedex, France

[65] Laboratoire de Physique Subatomique et de Cosmologie, CNRS/IN2P3, Université Joseph Fourier Grenoble I, Institut National Polytechnique de Grenoble, 53 rue des Martyrs, 38026 Grenoble Cedex, France

[66] Laboratoire de l'Accélérateur Linéaire, Université Paris-Sud 11, CNRS/IN2P3, Orsay, France

[67] Lawrence Berkeley National Laboratory, Berkeley, California, USA

[68] Max-Planck-Institut für Astrophysik, Karl-Schwarzschild-Str. 1, 85741 Garching, Germany

[69] Max-Planck-Institut für Extraterrestrische Physik, Giessenbachstraße, 85748 Garching, Germany

[70] Niels Bohr Institute, Blegdamsvej 17, Copenhagen, Denmark

[71] Observational Cosmology, Mail Stop 367-17, California Institute of Technology, Pasadena, CA, 91125, USA

[72] Optical Science Laboratory, University College London, Gower Street, London, UK

[73] SISSA, Astrophysics Sector, via Bonomea 265, 34136, Trieste, Italy

[74] School of Physics and Astronomy, Cardiff University, Queens Buildings, The Parade, Cardiff CF24 3AA, UK

[75] Space Research Institute (IKI), Russian Academy of Sciences, Profsoyuznaya Str, 84/32, Moscow 117997, Russia

[76] Space Sciences Laboratory, University of California, Berkeley, California, USA

[77] Stanford University, Dept of Physics, Varian Physics Bldg, 382 via Pueblo Mall, Stanford, California, USA

[78] Tartu Observatory, Toravere, Tartumaa, 61602, Estonia

[79] Tuorla Observatory, Department of Physics and Astronomy, University of Turku, Väisäläntie 20, 21500 Piikkiö, Finland

[80] UPMC Univ Paris 06, UMR7095, 98bis boulevard Arago, 75014 Paris, France

[81] Universität Heidelberg, Institut für Theoretische Astrophysik, Albert-Überle-Str. 2, 69120 Heidelberg, Germany

[82] Université de Toulouse, UPS-OMP, IRAP, 31028 Toulouse Cedex 4, France

[83] University Observatory, Ludwig Maximilian University of Munich, Scheinerstrasse 1, 81679 Munich, Germany

[84] University of Granada, Departamento de Física Teórica y del Cosmos, Facultad de Ciencias, Granada, Spain

[85] Warsaw University Observatory, Aleje Ujazdowskie 4, 00-478 Warszawa, Poland